



Solar light-facilitated oxytetracycline removal from the aqueous phase utilizing a $\text{H}_2\text{O}_2/\text{ZnWO}_4/\text{CaO}$ catalytic system

Pankaj Raizada^{a,*}, Pooja Shandilya^a, Pardeep Singh^a, Pankaj Thakur^{a,b}

^a School of Chemistry, Faculty of Basic Science, Shoolini University, Solan, Himachal Pradesh 173212, India

^b Center for Advanced Biomaterials for Healthcare, Istituto Italiano Di Tecnologia, 80125 Naples, Italy

Received 11 April 2016; received in revised form 8 June 2016; accepted 14 June 2016

Abstract

A CaO-supported ZnWO_4 nanocomposite (ZnWO_4/CaO) was successfully synthesized using a novel hydrothermal method and was characterized by scanning electron microscopy (SEM), tunnelling electron microscopy (TEM), X-ray diffraction (XRD), electron diffraction X-ray (EDX), Fourier transform infrared spectroscopy (FTIR) and UV–visible (UV–vis) spectral analysis. The ZnWO_4/CaO composites exhibited rod-like morphologies with variable lengths from 45 nm to 147 nm and diameters from 26 nm to 36 nm. The catalytic efficiency of the synthesized ZnWO_4/CaO composites was displayed for the photodegradation of oxytetracycline (OTC) antibiotic from the aqueous phase. The synergistic degradation of OTC was investigated in the presence of H_2O_2 and ZnWO_4/CaO . The rate of photodegradation followed pseudo-first-order kinetics. The antibiotic removal was strongly influenced by the catalyst loading, H_2O_2 concentration, pH and OTC concentration. Using a solar/ $\text{H}_2\text{O}_2/\text{ZnWO}_4/\text{CaO}$ catalytic system, 85% COD removal was attained for OTC degradation in 210 min. The oxidative degradation occurred through hydroxyl radicals. The prepared nanocomposites possessed high recyclability and were easily separated from the aqueous solution by a simple sedimentation process.

© 2016 Taibah University. Production and hosting by Elsevier B.V. This is an open access article under the CC BY-NC-ND license (<http://creativecommons.org/licenses/by-nc-nd/4.0/>).

Keywords: Supported- ZnWO_4 ; H_2O_2 ; Enhanced-photocatalysis; Antibiotic removal; Kinetics

1. Introduction

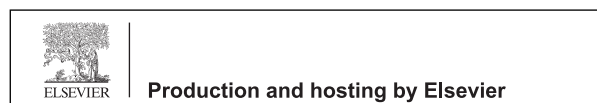
Antibiotics represent a class of chemicals that are used worldwide in pharmaceuticals and personal care

products (PPCPs) and are toxic to the ecosystem [1,2]. Tetracycline (TC) as an important member of the antibiotic group is used for disease treatment, prevention and growth promoters [3,4]. Among all of the antibiotics, oxytetracycline (OTC) is one of the most frequently detected tetracyclines in water bodies and sediments [5,6]. The traditional methods of wastewater decontamination, such as coagulation, flocculation, precipitation, adsorption, membrane separation techniques and aerobic biological treatment, prove inefficient for the complete degradation of organic pollutants into innocuous products but have been used for the removal of antibiotics from wastewater [7,8].

* Corresponding author. Fax: +91 1792 30800.

E-mail address: pankajchem1@gmail.com (P. Raizada).

Peer review under responsibility of Taibah University.



<http://dx.doi.org/10.1016/j.jtusci.2016.06.004>

1658-3655 © 2016 Taibah University. Production and hosting by Elsevier B.V. This is an open access article under the CC BY-NC-ND license (<http://creativecommons.org/licenses/by-nc-nd/4.0/>).

Please cite this article in press as: P. Raizada, et al. Solar light-facilitated oxytetracycline removal from the aqueous phase utilizing a $\text{H}_2\text{O}_2/\text{ZnWO}_4/\text{CaO}$ catalytic system, J. Taibah Univ. Sci. (2016), <http://dx.doi.org/10.1016/j.jtusci.2016.06.004>

Photocatalytic degradation of organic pollutants by semiconductor photocatalysts has emerged as a potential technology for water purification. The advanced oxidation process is a promising technology due to its low cost, simplicity and high efficiency as well as its ability to generate no secondary pollution [9–11]. When a photocatalyst is excited with photons of energy equal to or higher than its band gap energy, electrons (e^-) and hole (h^+) pairs are created. The photogenerated holes migrate to the hydroxylated surface and produce highly reactive OH^\bullet species (oxidation potential = 2.8 eV). The oxidative degradation occurs through hydroxyl radicals that degrade the organic/inorganic pollutants present in the aqueous phase [12].

Binary metal oxides such as TiO_2 , ZnO , Cu_2O , WO_3 , V_2O_5 , NiO , ZrO_2 , and CeO_2 have been synthesized and investigated for photocatalytic water purification [12,13]. In this context, as a member of the metal tungstate family, $ZnWO_4$ is emerging as a promising photocatalyst due to its non-toxicity, low cost, high chemical stability and visible light activity [14]. He et al. prepared a $Bi_2WO_6/ZnWO_4$ composite via a simple hydrothermal method involving the growth of Bi_2WO_6 nanoparticles on $ZnWO_4$ nanorods [15]. Zhang et al. studied the band structure, morphology and photocatalytic activity of $ZnWO_4$ for the photodegradation of rhodamine blue dye from the aqueous phase [16]. Bai et al. explored the visible light activity of graphene– $ZnWO_4$ nanocomposites for the degradation of methylene blue dye [17].

The adsorption of pollutant onto the catalyst surface is required for the efficient photodegradation process in the aqueous phase [7,10,12]. However, the large-scale application of $ZnWO_4$ is hindered due to the low adsorptional photocatalytic activity [4]. Therefore, the improvement of the adsorptional photocatalytic activity of $ZnWO_4$ still poses a challenge. Calcium oxide (CaO) is used as an industrial compound, catalyst, toxic-waste remediation agent, an additive in refractory processes and for other fundamental applications [18]. Considerable attention has been focused on calcium oxide because it has high CO_2 adsorption capacity and high raw material availability (e.g., limestone) at a low cost [19]. H_2O_2 is the simplest oxidant that reduces a low concentration of pollutants present in wastewater [20]. Under UV light, H_2O_2 decomposes and generates OH^\bullet radicals, which are responsible for the destruction of target pollutants. The use of H_2O_2 becomes more effective when used in conjunction with other reagents or energy sources capable of dissociating it to generate OH^\bullet radicals [21].

The current studies have emphasized the applicability of $ZnWO_4/CaO$ composites as a photocatalyst for

the degradation of oxytetracycline in the aqueous phase. A facile hydrothermal method was used to synthesize $ZnWO_4/CaO$ composites. The $ZnWO_4/CaO$ catalyst was characterized by scanning electron microscopy (SEM), transmission electron microscopy (TEM), X-ray diffraction (XRD), energy dispersive X-ray analysis (EDX), Fourier transform infrared (FTIR) and ultraviolet–visible (UV–vis) spectral techniques. The influence of various reaction parameters was evaluated on the photodegradation of OTC. The synergistic effect of adsorption and photocatalysis with the most plausible mechanism on the photodegradation of OTC was also explored. The use of solar light was preferred over an expensive artificial source. Additionally, the recovery and recyclability of the $ZnWO_4/CaO$ catalyst was examined.

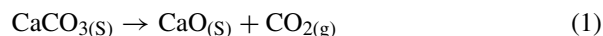
2. Experimental

2.1. Materials

All of the chemicals used in this study were of analytical grade. Oxytetracycline antibiotic, sodium tungstate dihydrate ($Na_2WO_4 \cdot 2H_2O$) and zinc nitrate hexahydrate [$Zn(NO_3)_2 \cdot 6H_2O$] were purchased from Sigma Aldrich. Hen eggshells were collected from a local market in Solan, Himachal Pradesh, India. All of the solutions were prepared in double distilled water.

2.2. Preparation of CaO

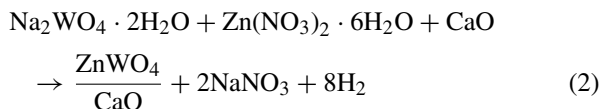
The hen eggshells were washed with distilled water to remove any adhered impurities. The washed hen eggshells were boiled and heated at 800 °C for 2 h to obtain CaO (Eq. (1)). The obtained CaO was dried, ground and sieved to a fragment size less than 200 mesh and preserved for further use:



2.3. Preparation of $ZnWO_4/CaO$ composites

The $ZnWO_4/CaO$ composites were prepared with little modification in the hydrothermal method [22]. In a typical synthesis, a 0.1 M of sodium tungstate dehydrate solution and 0.1 M of zinc nitrate hexahydrate were mixed in 50 ml of distilled water and sonicated for 30 min. After sonicating the mixture, 6.272 g of CaO was added with continuous stirring for 4 h at 70 °C (Eq. (2)). The precipitates were filtered, washed with ethanol and heated in a muffle furnace at 400 °C for 2 h. The obtained

composites were levelled as ZnWO₄/CaO and preserved for further use:



2.4. Photocatalytic activity

Photocatalytic, photolytic and dark experiments were executed in a double-walled Pyrex vessel (7.5-cm high × 6-cm wide) surrounded by a thermostatic water circulation arrangement (30 ± 0.3 °C). During the equilibration experiments, the slurry composed of OTC and the ZnWO₄/CaO catalyst suspension was continuously stirred and kept under solar light [23,24]. At specific time intervals, an aliquot (3 ml) was withdrawn and centrifuged for 2 min to remove the catalyst particles from the aliquot. The absorbance of OTC was observed at 280 nm. The solar light intensity was measured by a digital lux-metre (35 × 10³ ± 1000 lx). Photocatalytic experiments were performed between March and May 2014 (11 am–2 pm). All of the experiments were undertaken in triplicate with errors below 5% and with the average values reported. The chemical oxygen demand (COD) was measured by the closed reflux method. The unreacted oxidant was determined by titrating the sample with ferrous ammonium sulphate using a ferroin indicator. The removal efficiency was calculated using Eq. (3) [25]:

$$\% \text{removal efficiency} = \frac{C_0 - C_t}{C_0} \quad (3)$$

where C_0 is the initial concentration of sample/COD and C_t /COD is the instant concentration of sample/COD.

The kinetics of OTC degradation was explained by pseudo-first-order kinetics. The rate constant (k) and half-life period ($t_{1/2}$) were calculated using Eqs. (4) and (5), respectively [25]:

$$k = 2.303 \times \text{slope} \quad (4)$$

$$t_{1/2} = \frac{0.693}{k} \quad (5)$$

where the slope was obtained from the plot of $\ln(c)$ versus ' t '.

3. Results and discussion

3.1. Characterization of the ZnWO₄/CaO composites

Fig. 1 depicts the SEM images of pure CaO (a–b) and ZnWO₄/CaO composites (c–d). CaO exhibits a porous surface, which facilitates the adsorption of organic/inorganic molecules. Fig. 1(c) and (d) reveals that ZnWO₄ nanoparticles were unevenly distributed on the surface of the pure 200-nm CaO microsphere. The incorporation of ZnWO₄ onto the CaO surface reduced the porosity of the composite.

The TEM images of the ZnWO₄/CaO composites are shown in Fig. 2(a)–(c). These images indicate that the nanocomposite exhibits a rod-like structure, with spherical particles arranged in an irregular fashion [26]. The particle length varied from 45 nm to 147 nm and the diameter from 26 nm to 36 nm. The dark surface in the images reveals the attachments of ZnWO₄ onto the light grey surface of CaO.

Fig. 3(a) shows the UV–vis absorption spectra of the ZnWO₄/CaO composite in ethanol. The absorption edge was located at approximately 360 nm. The band gap of the ZnWO₄/CaO composite was calculated using the Tauc relationship [12]:

$$\alpha h\nu = B(h\nu - E_g)^n \quad (6)$$

where α is the absorption coefficient = 2.303 A/l, E_g is the optical band gap, B is the band tailing parameter, $h\nu$ is the photon energy and $n = 1/2$ for a direct band gap. The optical band gap is determined by extrapolating the straight portion of the curve between $(\alpha h\nu)^2$ and $h\nu$ when $\alpha = 0$. The band gap of the ZnWO₄/CaO composite was 3.44 eV.

Fig. 3(b) shows the XRD diffractogram of the CaO and ZnWO₄/CaO composites. The diffraction pattern of the prepared CaO corresponded to the (111), (220) and (311) planes, which were in good agreement with the standard JCPDS file (No. 82-1691) [28]. The planes of (100), (111), (021), (200), (200), (220), (041) and (311) confirmed the presence of the ZnWO₄/CaO composite according to standard JCPDS (No. 15-0774) and (No. 82-169) [27,28]. The characteristic peaks of CaO were observed at 47.123° and 84.743°. The diffraction peaks of the ZnWO₄/CaO composite were observed at 22.206° and 28.707°. These shifts of a few plane peaks were due to the attachment of ZnWO₄ to CaO. The semi-crystallites of the ZnWO₄/CaO composites were in the range of 26–50 nm.

Fig. 3(c) and (d) shows the EDX pattern of CaO and the ZnWO₄/CaO composites. The EDX spectrum

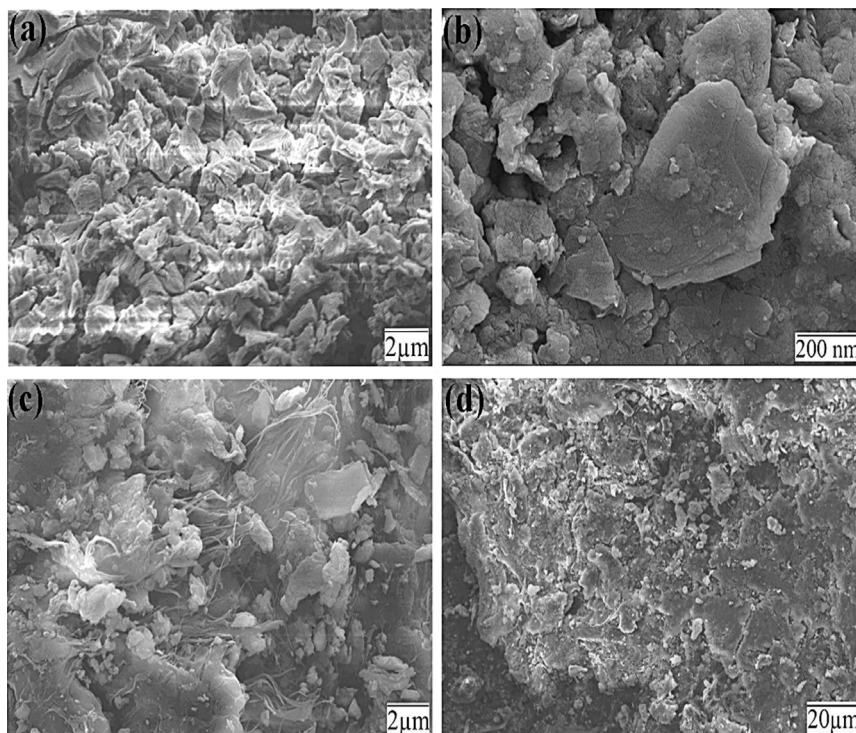


Fig. 1. (a, b) SEM image of pure CaO and (c, d) SEM images of ZnWO₄/CaO composites.

confirmed the presence of elements Ca, O, C in the CaO sample (Fig. 3(c)). The presence of the Ca, O, C, W and Zn elements indicated the successful preparation of ZnWO₄/CaO composites in Fig. 3(d).

Fig. 4 illustrates the IR spectra of CaO and the ZnWO₄/CaO composite. In the CaO spectrum, the peak at 712 cm⁻¹ was due to Ca–O bonding. The peaks at 2982 cm⁻¹, 2875 cm⁻¹, 2516 cm⁻¹ and 1798 cm⁻¹ were assigned to the amines and amides of the eggshell membrane [29]. The absorption peaks at 1417 cm⁻¹, 866 cm⁻¹ and 3420 cm⁻¹ corresponded to C–O and O–H bonds [30]. The peaks at 592 cm⁻¹ and 798 cm⁻¹ were due to the bending and stretching vibrations of W–O, respectively. The peak at 874 cm⁻¹ was ascribed to the bending and stretching vibrations of Zn–O–W [31]. The peaks at 1384 cm⁻¹, 1628 cm⁻¹ and 3411 cm⁻¹ were due to the O–H stretching and the H–O–H bending vibrations [32]. The weak absorption peaks at 2874 cm⁻¹ and 2985 cm⁻¹ were assigned to C–O vibrations [33].

3.2. OTC removal under different catalytic systems

Photocatalytic degradation of OTC was explored using different catalytic systems under solar light and in the dark. Under solar light, 85% of OTC was removed using the H₂O₂/ZnWO₄/CaO system (Fig. 5(a)), while

50% and 30% of OTC was removed utilizing the ZnWO₄ and H₂O₂ systems, respectively. In the absence of solar light, 45% and 43% of OTC was removed utilizing the H₂O₂/ZnWO₄/CaO and ZnWO₄/CaO systems, respectively (Fig. 5(b)). In the dark, H₂O₂ alone had no effect on OTC removal. The OTC removal followed the trend of H₂O₂/ZnWO₄/CaO (solar light) > ZnWO₄/CaO (solar light) > H₂O₂/ZnWO₄/CaO (dark) ≈ ZnWO₄/CaO (dark) > H₂O₂ (solar light) ≫ solar light ≈ H₂O₂ (dark). Under the given experimental conditions, the solar/H₂O₂/ZnWO₄/CaO system exhibited a higher efficiency for the removal of OTC.

To investigate the role of adsorption in photodegradation, OTC removal using solar/H₂O₂/ZnWO₄/CaO was investigated under three different conditions, i.e., adsorption in the dark (DA), equilibrium adsorption followed by photodegradation (A – P) and simultaneous adsorption and photocatalysis (A + P). Fig. 5(c) shows the removal efficiency of H₂O₂/ZnWO₄/CaO as a function of time using DA, A – P and A + P. The first portion of the graph displays the adsorption process in the dark using the H₂O₂/ZnWO₄/CaO/DA system, while the second fragment was ascribed to A – P and A + P under solar light. During the simultaneous adsorption and degradation process (A + P), 85% of OTC was decolorized in 210 min. Only 53% of OTC was removed during

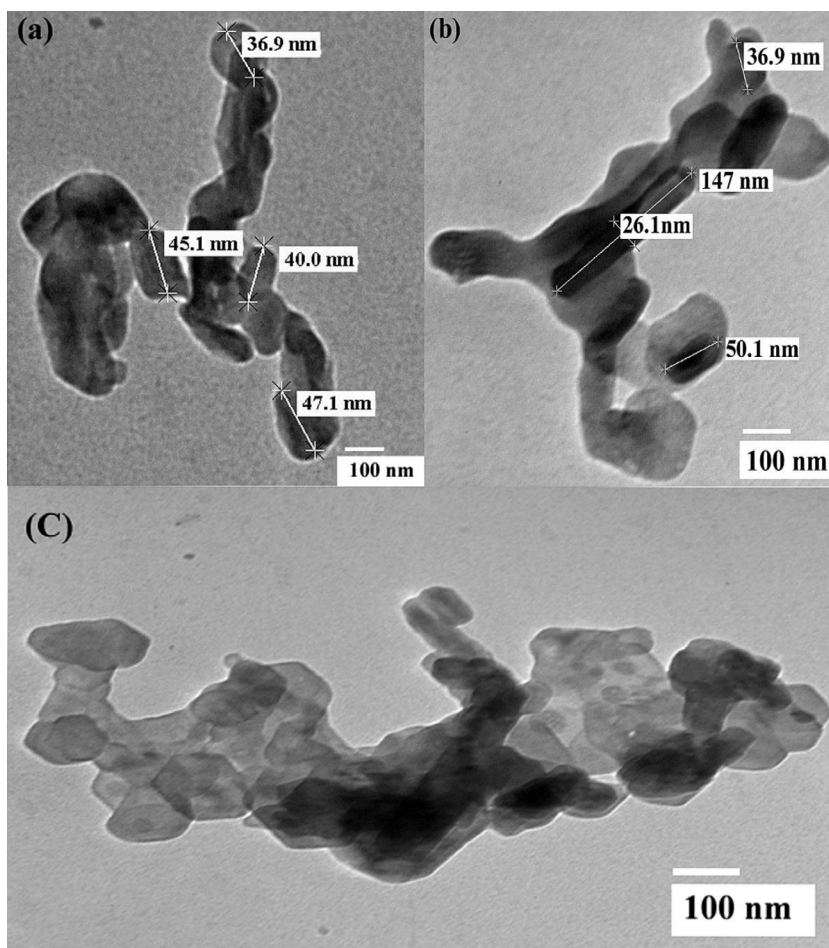


Fig. 2. TEM images of ZnWO_4/CaO composites.

the dark adsorption experiment. The efficiency of various catalytic systems for OTC removal followed the order of $\text{H}_2\text{O}_2/\text{CaO}/\text{A} + \text{P} > \text{Zr-TiO}_2/\text{CaO}/\text{A} - \text{P} > \text{Zr-TiO}_2/\text{CaO}/\text{DA}$. Furthermore, it can be noticed that OTC removal in the A + P system was higher than that for the A – P system. Our results for adsorption and degradation studies were comparable to the previous work by Shoun and co-workers [34]. In this work, the A – P system had a lower removal efficiency than that of DA due to the hindering effect of adsorption on the photocatalytic process. The three processes followed the efficiency order of $\text{A} + \text{P} > \text{DA} > \text{A} - \text{P}$. The solar/ $\text{H}_2\text{O}_2/\text{ZnWO}_4/\text{CaO}/\text{A} + \text{P}$ catalytic system was the most efficient photocatalytic system, and further OTC degradation studies were explored using this catalytic system. The photodegradation of OTC using the $\text{H}_2\text{O}_2/\text{ZnWO}_4/\text{CaO}$ catalytic system followed pseudo-first-order kinetics ($R^2 = 0.994$) with a rate constant of $4.6 \times 10^{-3} \text{ min}^{-1}$ (Fig. 5(c)).

3.3. Effect of reaction parameters on the activity of the solar/ $\text{H}_2\text{O}_2/\text{ZnWO}_4/\text{CaO}/\text{A} + \text{P}$ system

Fig. 6(a)–(d) depicts the influence of various reaction parameters, such as OTC concentration, catalyst loading, pH and H_2O_2 concentration, on the activity of the solar/ $\text{H}_2\text{O}_2/\text{ZnWO}_4/\text{CaO}/\text{A} + \text{P}$ system. Fig. 6(a) displays the effect of OTC concentration on the catalytic activity of the solar/ $\text{H}_2\text{O}_2/\text{ZnWO}_4/\text{CaO}$ system. Because the degradation rate is related to the probability of the formation of OH^\bullet radicals on the catalyst surface and the reaction of the radicals with OTC molecules, the OTC concentration was varied from $0.7 \times 10^{-4} \text{ M}$ to $9 \times 10^{-4} \text{ M}$. With an increase in OTC concentration from $0.7 \times 10^{-4} \text{ M}$ to $5.0 \times 10^{-4} \text{ M}$, the rate constant increased from $2 \times 10^{-4} \text{ s}^{-1}$ to $8.8 \times 10^{-4} \text{ s}^{-1}$. The increase in the rate constant was due to the higher availability of OTC molecules. The rate constant decreased with an increase in OTC concentration beyond

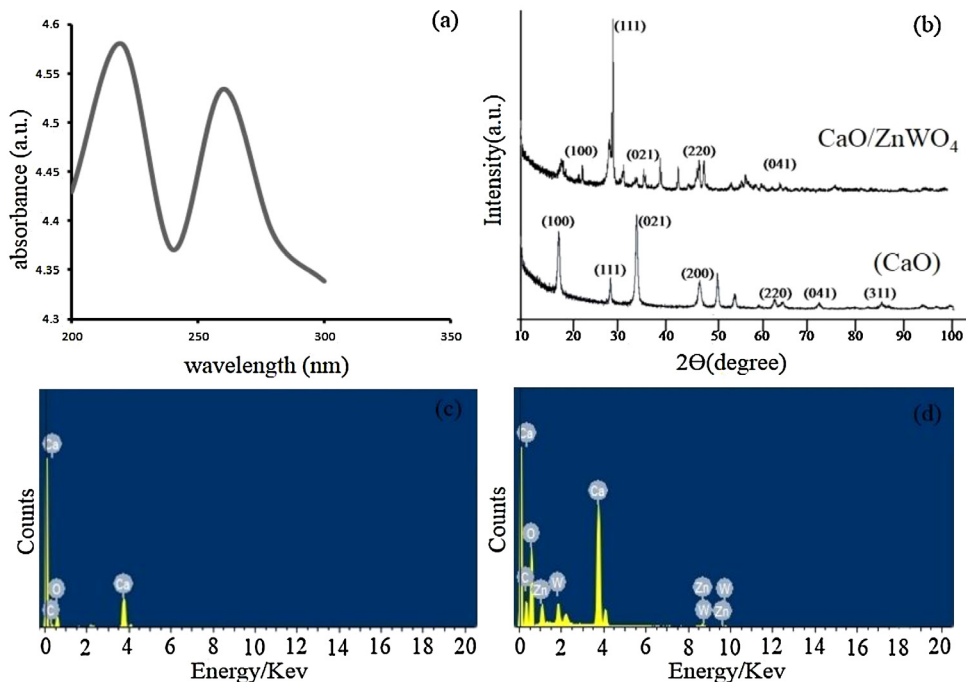


Fig. 3. (a) UV–vis absorbance spectra of ZnWO_4/CaO composites. (b) X-ray diffraction pattern of pure CaO and ZnWO_4/CaO composites. (c, d) EDX pattern of pure CaO and ZnWO_4/CaO composites.

5.0×10^{-4} M. This decrease was because OTC acted as a filter for incident radiation and reduced the photoactive volume [10,34]. Second, the excessive adsorption of OTC molecules on the catalyst surface hindered the competitive adsorption of OH^\bullet ions, thus reducing the rate of OH^\bullet radical formation [10,34].

The effect of catalyst loading was investigated by varying the catalyst dose from 10 mg/50 ml to 130 mg/50 ml (Fig. 6(b)). The rate constant increased from $1.0 \times 10^{-2} \text{ s}^{-1}$ to $4.0 \times 10^{-2} \text{ s}^{-1}$ with an increase in catalyst loading from 10 mg/50 ml to 90 mg/50 ml. The higher rate constant was due to a higher OH^\bullet

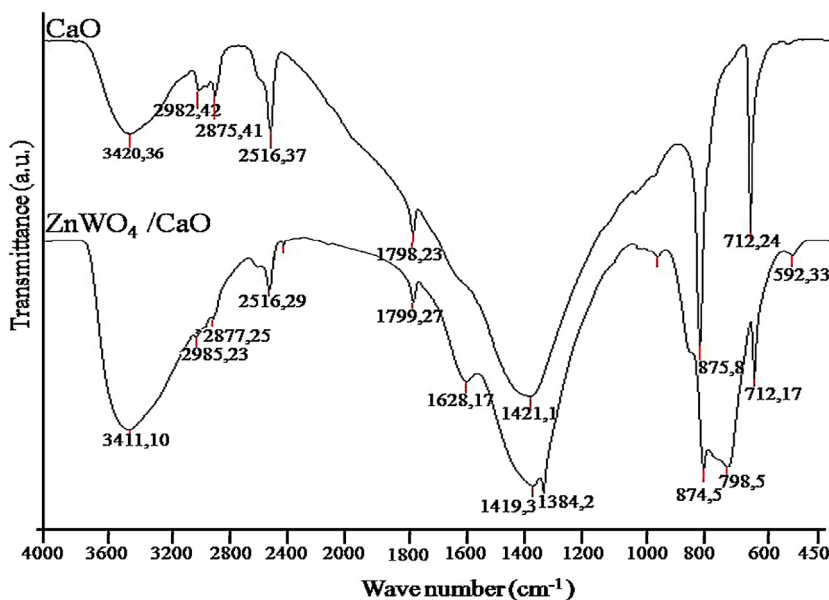


Fig. 4. FTIR spectra of pure CaO and ZnWO_4/CaO composites.

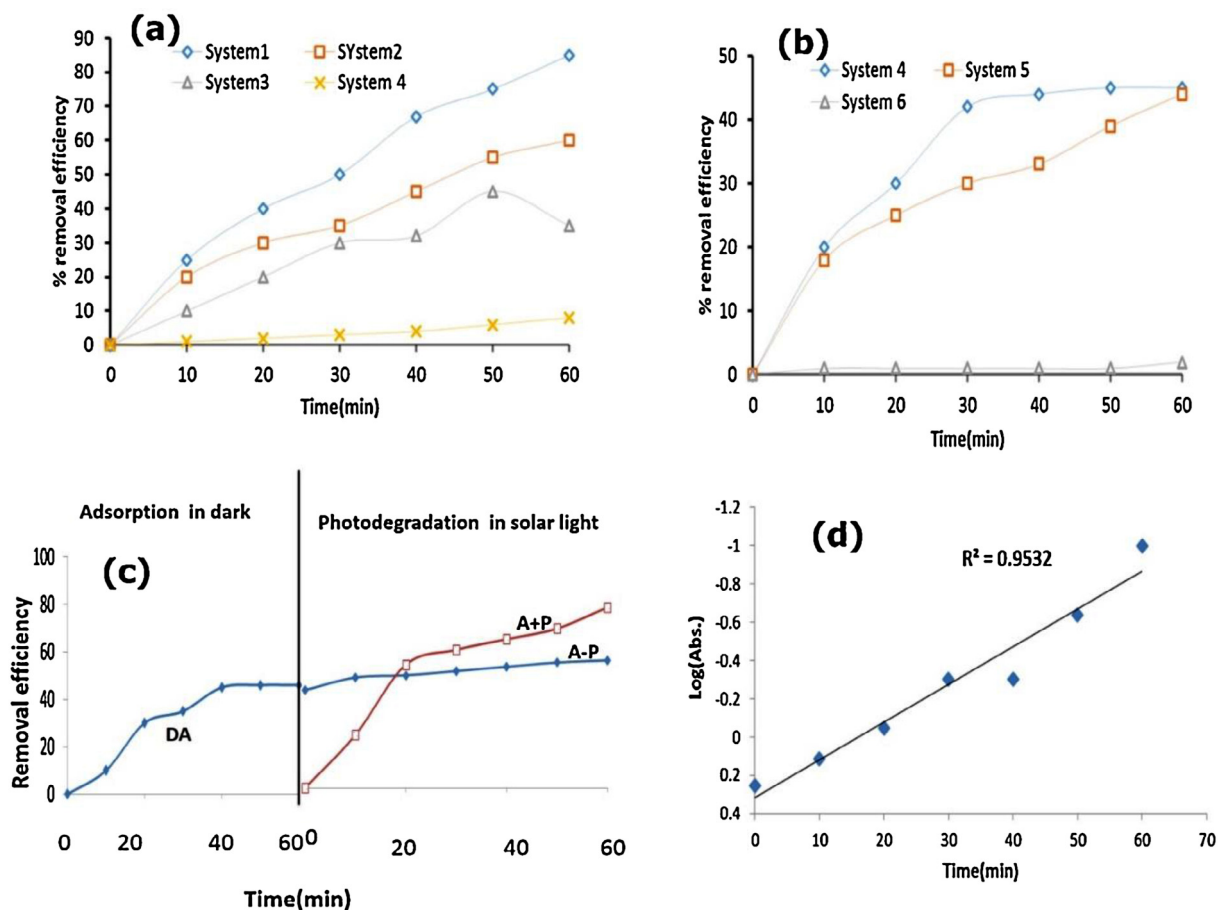


Fig. 5. (a, b) Time profile of OTC degradation in the $H_2O_2/CaO/ZnWO_4$ system under different reaction conditions (a) solar and (b) in the dark. (c) Time profile for adsorptional photocatalytic degradation of OTC. (d) The plot of $\log(\text{absorbance})$ vs. time. Experimental conditions: $[OTC] = 1 \times 10^{-4}$ M, $[H_2O_2] = 1 \times 10^{-4}$ M, Catalyst dosage = 50 mg/50 ml, pH 5, temperature = 30 ± 0.3 °C and time = 70 min.

formation and a greater availability of catalyst surface for adsorption of OTC molecules. However, above the optimal concentration, excess loading reduced the photoactivity due to screening of solar light by the higher catalyst dose [10,34].

Fig. 6(c) describes the effect of H_2O_2 concentration on the photodegradation of OTC. The rate constant increased from $4.90 \times 10^{-2} \text{ min}^{-1}$ to $8.5 \times 10^{-2} \text{ min}^{-1}$ with an increase in the H_2O_2 concentration from 0.7×10^{-4} M to 1.0×10^{-4} M. This result occurred because H_2O inhibited electron-hole recombination by accepting photogenerated electrons from the conduction band of the semiconductor. OH^\bullet radicals were also produced by photolysis of H_2O_2 according to Eqs. (7) and (8) [10,34]:



However, beyond the optimal concentration of H_2O_2 , the rate constant decreased due to the consumption of hydroxyl radicals. Above the optimal concentration, H_2O_2 became a scavenger for valence band holes and OH^\bullet to form HO_2^\bullet radicals, which are much weaker oxidants than OH^\bullet radicals [35]. The effect of pH on OTC degradation is shown in Fig. 6(d). Initially, the rate constant increased from $1.0 \times 10^{-2} \text{ min}^{-1}$ to $4.0 \times 10^{-2} \text{ min}^{-1}$ with an increase in pH from 1 to 5. At pH 2, OTC was fully protonated as H_3OTC^+ [35,36]. At low pH, the surface of $ZnWO_4/CaO$ was positively charged, resulting in a lower adsorption of OTC onto the catalyst surface. However, the majority of OTC changed to the zwitterionic form (H_2OTC^\pm) at pH 5.5 [35,36], resulting in higher adsorption of OTC onto the catalyst surface, leading to an increased rate of OTC photodegradation. At pH values of 8.5 and 11, OTC mainly existed as $HOTC^-$ and OTC^{2-} , respectively [35,36]. Above pH 7, the negatively charged catalyst surface caused poor

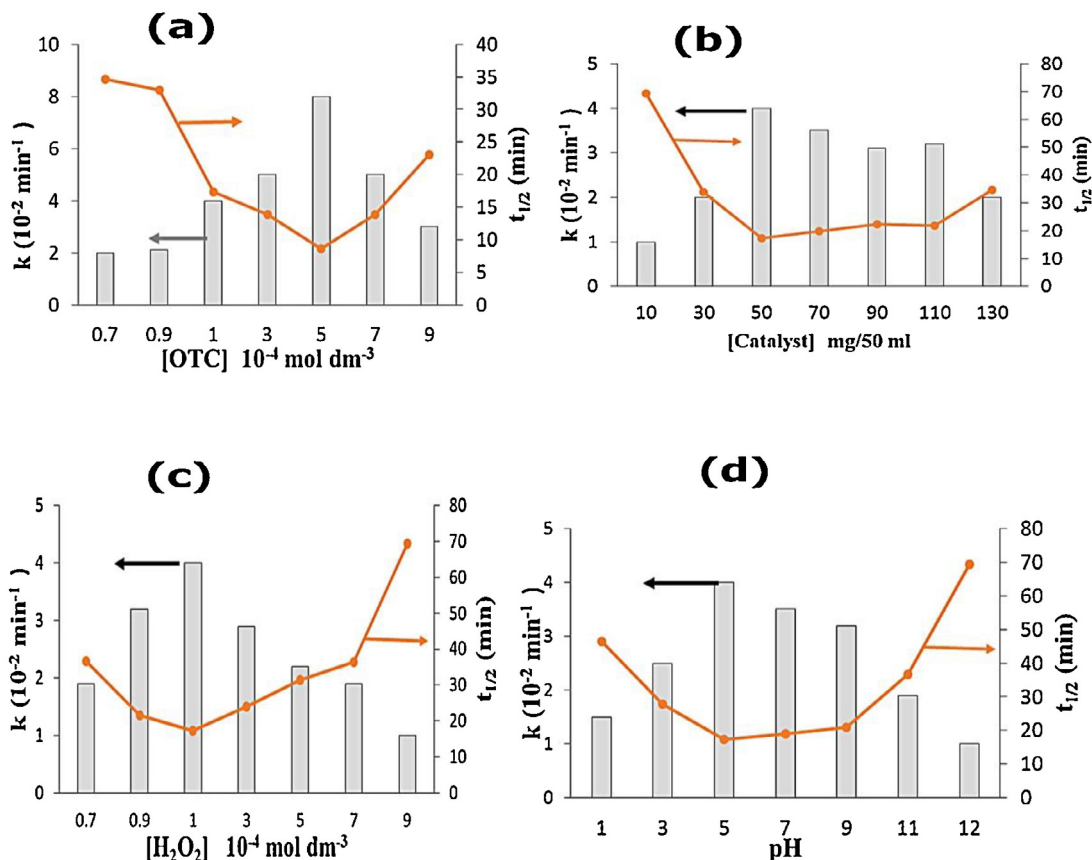


Fig. 6. (a–d) Effect of different reaction parameters, OTC (a), catalyst (b), H_2O_2 (c), pH (d) on OTC removal. Reaction conditions $[\text{OTC}] = 1 \times 10^{-4} \text{ M}$, catalyst dosage = 50 mg/50 ml, $[\text{H}_2\text{O}_2] = 1 \times 10^{-4} \text{ M}$, pH 5, temperature = $30 \pm 0.3 \text{ }^\circ\text{C}$, reaction time = 60 min and solar light intensity = $35 \times 10^3 \pm 1000 \text{ lx}$.

adsorption of HOTC^- and OTC^{2-} . At lower pH values, ZnWO_4 dissolved to form salts, and at a higher pH, they form zincates such as $[\text{Zn}(\text{OH})_4]^{2-}$ [5,35,37].

3.4. Proposed mechanism for OTC degradation under solar/ H_2O_2 / ZnWO_4 / CaO /A + P

Generally, photocatalytic degradation processes occur through hydroxyl radical-mediated oxidation of organic molecules (oxidation potential – 2.8 eV). To explore the role of $\bullet\text{OH}$ radicals, OTC degradation experiments were performed with isopropanol. Isopropanol containing α -hydrogen is highly reactive with OH^\bullet and is has a low reactivity with the O_2^- species. Buxton and co-workers reported the high second order rate constant ($6 \times 10^9 \text{ M}^{-1} \text{ s}^{-1}$) of isopropanol with OH^\bullet radicals [37]. The rate of OTC removal was significantly reduced due to presence of isopropanol; only 7% of OTC was removed in the presence of isopropanol due to the quenching of hydroxyl radicals. These results

indicated that degradation mainly occurred via a OH^\bullet radical-assisted oxidative pathway.

The OTC degradation was confirmed by measuring the COD value at different time intervals. It was found that 8% of OTC was degraded in 60 min using the solar/ H_2O_2 / ZnWO_4 /A + P catalytic system, and OTC was completely degraded in 210 min (Fig. 7). To further explore the mineralization kinetics, the power law model was explored. The real degradation process can be represented as the combination of two parallel branches, namely, photocatalysis and photolysis (Eq. (9)):

$$R = -\frac{dc}{dt} = R_1 + R_2 \quad (9)$$

where R , R_1 and R_2 are the net photodegradation, photocatalysis and photolysis rates, respectively. In the present study, photolysis has no significant effect on the antibiotics' degradation. Therefore, only photocatalysis was considered as the dominant process during long-term photocatalysis for ten hours. Here, the power law model was applied to explore the kinetics of the OTC

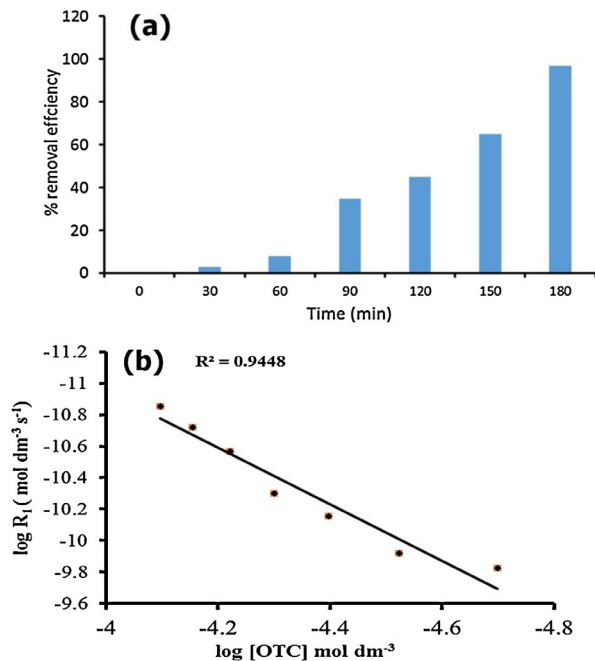


Fig. 7. (a) COD removal efficiency and (b) mineralization kinetics during degradation of OTC. Reaction conditions [OTC] = 1×10^{-4} M, catalyst dosage = 50 mg/50 ml, $[H_2O_2] = 1 \times 10^{-4}$ M, pH 5, temperature = 30 ± 0.3 °C and solar light intensity = $35 \times 10^3 \pm 1000$ lx.

mineralization process using the $ZnWO_4/CaO/A + P$ catalytic system (Eq. (10)):

$$R = k_1[ANT]^{n_1} \quad (10)$$

where k_1 is the rate constant for photocatalysis and n_1 denotes the order of the reaction for photocatalysis. To determine the appropriate parameters, the differential method of data analysis was applied to Eq. (10). Fig. 7(a) represents the goodness of fit of the rate in Eq. (10). The reaction order (n_1) was determined as 1.54. $H_2O_2/ZnWO_4/CaO$ catalytic systems had a rate constant of $4.57 \times 10^{-8} (\text{mol dm}^{-3})^{-0.54} \text{ min}^{-1}$. These results clearly indicated that long-term degradation did not follow simple pseudo-first-order kinetics. The degradation process tends to be slower with increased degradation time, and the overall process of mineralization is complex.

During the photocatalytic process, the illumination of $ZnWO_4/CaO$ produced conduction band electrons (e_{CB}^-) and valance band holes (h_{VB}^+) (Eqs. (9)–(16)). H_2O_2 mainly contributed to the degradation process by acting as an electron scavenger of valance band holes, leading to the lower electron–hole pair recombination. The active OH^\bullet and ($O_2^{\bullet-}$) were also generated directly during illumination of $ZnWO_4/CaO$ [4]. At $pH \approx 5$, $HOTC^-$ was excited to a singlet state, which

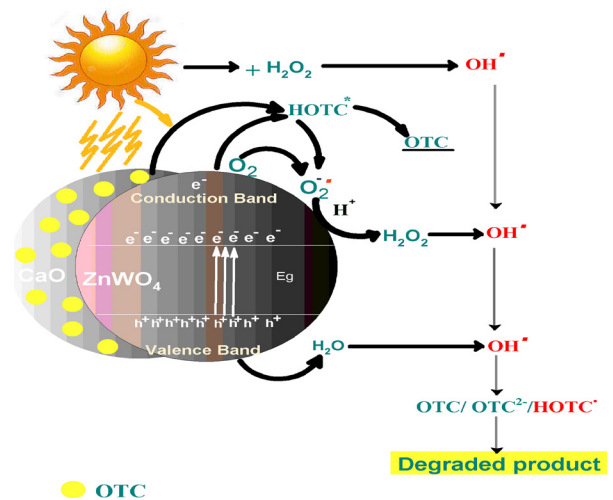
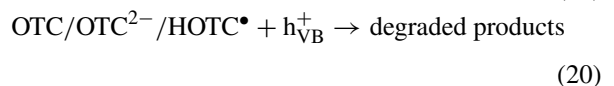
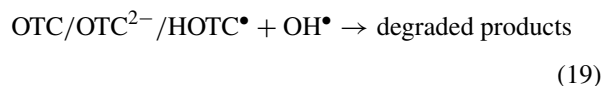
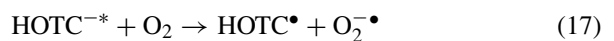
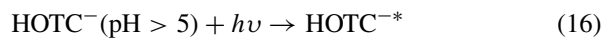
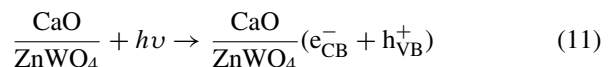


Fig. 8. The proposed mechanism for OTC degradation under the solar/ $H_2O_2/ZnWO_4/CaO$ system.

crossed to the triplet state $HOTC^{-*}$ via an intersystem crossing mechanism [34]. The triplet state $HOTC^{-*}$ caused the injection of electrons in the conduction band to generate superoxide anion radicals ($O_2^{\bullet-}$) [34]. $HOTC^-$ also acted as an electron scavenger for conduction band electrons. Third, $HOTC^{-*}$ also acted as a sensitizer during the solar photocatalytic removal of OTC [34]. The produced active species led to oxidative degradation of OTC [32,34,37]. The overall mechanism was described by Eqs. (11)–(20) (Fig. 8):



Recycling efficiency is one of most crucial factors for an efficient photocatalytic process. The recycling

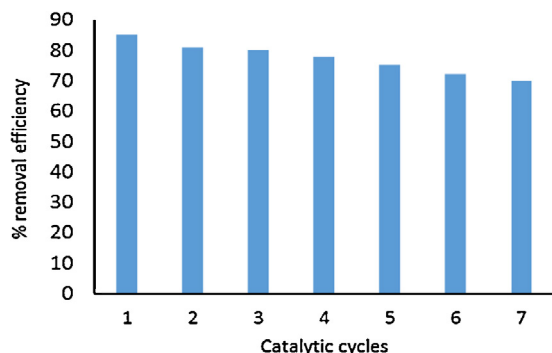


Fig. 9. Recycle catalytic activity of ZnWO_4/CaO . Reaction conditions: $[\text{OTC}] = 1 \times 10^{-4} \text{ M}$, $[\text{H}_2\text{O}_2] = 1 \times 10^{-4} \text{ M}$, catalyst dosage = 50 mg/50 ml, pH 5 and temperature = $30 \pm 1^\circ \text{C}$, reaction time = 60 min and solar light intensity = $35 \times 10^3 \pm 1000 \text{ lx}$.

efficiency of the ZnWO_4/CaO composites was explored for seven successive cycles of OTC removal (Fig. 8). During each run, the catalyst was separated from the solution through centrifugation followed by sedimentation. The efficiency of the ZnWO_4/CaO system was reduced to 70% from 85%. The study revealed that ZnWO_4/CaO composites were easily recycled after seven catalytic cycles, indicating the reusability of ZnWO_4/CaO composites during the photodegradation process (Fig. 9).

4. Conclusions

In this study, the photocatalytic activity of the $\text{H}_2\text{O}_2/\text{ZnWO}_4/\text{CaO}$ system was investigated for the degradation of OTC from an aqueous system. The successful formation of the ZnWO_4/CaO composite was ascertained by SEM TEM, EDX XRD, FTIR and UV–vis spectral analysis. The solar/ $\text{H}_2\text{O}_2/\text{ZnWO}_4/\text{CaO}$ catalytic system was the most efficient for OTC degradation. The photodegradation was higher during a simultaneous adsorption and photocatalytic process (A + P). The degradation of OTC was optimal at pH 5. The rate of the reaction was maximal with a 50 mg/50 ml ZnWO_4/CaO loading and $5.0 \times 10^{-4} \text{ M}$ of OTC concentration. Under solar light, H_2O_2 displayed a synergistic effect in conjunction with the ZnWO_4/CaO composites.

References

[1] J.C. Madden, S.J. Enoch, M. Hewitt, M.T.D. Cronin, Pharmaceuticals in the environment: good practice in predicting acute ecotoxicological effects, *Toxicol. Lett.* 185 (2009) 85–101.
 [2] S. Schnell, N.C. Bols, C. Barata, C. Porte, Single and combined toxicity of pharmaceuticals and personal care products (PPCPs)

on the rainbow trout liver cell line RTL-W1, *Aquat. Toxicol.* 93 (2009) 244–252.
 [3] C. Gu, K.G. Karthikeyan, Interaction of tetracycline with aluminum and iron hydrous oxides, *Environ. Sci. Technol.* 39 (2005) 2660–2667.
 [4] J. Jeong, W. Song, W.J. Cooper, J. Jung, J. Greaves, Degradation of tetracycline antibiotics mechanisms and kinetic studies for advanced oxidation/reduction processes, *Chemosphere* 78 (2010) 533–540.
 [5] B.J. Richardson, P.K.S. Lam, M. Martin, Emerging chemicals of concern pharmaceuticals and personal care products (PPCPs) in Asia, with particular reference to Southern China, *Mar. Pollut. Bull.* 50 (2005) 913–920.
 [6] A.J. Watkinson, E.J. Murby, D.W. Kolpin, S.D. Costanzo, The occurrence of antibiotics in an urban watershed: from wastewater to drinking water, *Sci. Total Environ.* 407 (2009) 2711–2723.
 [7] P. Raizada, P. Singh, A. Kumar, B. Pare, S.B. Jonnalagadda, Zero valent iron-brick grain nanocomposite for enhanced solar-Fenton removal of malachite green, *Sep. Purif. Technol.* 133 (2014) 429–437.
 [8] T. Robinson, G. McMullan, R. Marchant, P. Nigam, Remediation of dyes in textile effluent: a critical review on current treatment technologies with a proposed alternative, *Bioresour. Technol.* 77 (2001) 247–255.
 [9] D. Bahnemann, Photocatalytic water treatment: solar energy application, *Sol. Energy* 77 (2004) 445–459.
 [10] P. Raizada, S. Gautam, B. Priya, P. Singh, Preparation and photocatalytic activity of hydroxyapatite supported BiOCl nanocomposite for oxytetracycline removal, *Adv. Mater. Lett.* 7 (4) (2016) 312–318.
 [11] P. Singh, P. Raizada, Solar-Fenton removal of malachite green with novel Fe0-activated carbon nanocomposite, *Appl. Catal. A: Gen.* 476 (2014) 9–18.
 [12] P. Raizada, P. Singh, A. Kumar, G. Sharma, B. Pare, S.B. Jonnalagadda, P. Thakur, Solar photocatalytic activity of nano-ZnO supported on activated carbon or brick grain particles: role of adsorption in dye degradation, *Appl. Catal. A* 486 (2014) 159–169.
 [13] R. Asahi, T. Morikawa, T. Ohwaki, K. Aoki, Visible-light photocatalysis in nitrogen-doped titanium, *Science* 293 (2001) 269–271.
 [14] H. Fu, J. Lin, L. Zhang, Photocatalytic activities of novel ZnWO_4 catalyst prepared by hydrothermal process, *Appl. Catal. A* 306 (2006) 58–67.
 [15] D. He, L. Wang, D. Xu, J. Zhai, D. Wang, Investigation of photocatalytic activity over $\text{Bi}_2\text{WO}_6/\text{ZnWO}_4$ composite under UV light and its photo induced charge transfer properties, *ACS Appl. Mater. Interfaces* 3 (2011) 3167–3171.
 [16] C. Zhang, H. Zhang, K. Zhang, X. Li, Q. Leng, C. Hu, Photocatalytic activity of ZnWO_4 , band structure, morphology and surface modification, *ACS Appl. Mater. Interfaces* 6 (2014) 14423–14432.
 [17] X. Bai, L. Wang, Y. Zhu, Visible photocatalytic activity enhancement of ZnWO_4 by graphene hybridization, *ACS Catal.* 2 (2012) 2769–2778.
 [18] B.K. Olga, L. Isabelle, V. Alexander, Alkaline-earth oxide nanoparticles obtained by aerogel methods: characterization and rational for unexpectedly high surface chemical, *Chem. Mater.* 9 (1997) 2468–2472.
 [19] Z.H. Lee, K.T. Lee, S. Bhatia, A.R. Mohamed, Post-combustion carbon dioxide capture: evolution towards utilization of nanomaterials, *Renew. Sust. Energy Rev.* 16 (2012) 2599–2609.

- [20] E. Neyens, J. Baeyens, A review of classic Fenton's peroxidation as an advanced oxidation technique, *J. Hazard. Mater.* 98 (2003) 33–50.
- [21] D. Robert, S. Parra, C. Pulgarin, A. Hrzton, J.V. Weber, Chemisorption of phenols and acids on TiO₂ surface, *Appl. Surf. Sci.* 167 (2000) 51–58.
- [22] P. Singh, P. Raizada, P. Thakur, Preparation of BSA-ZnWO₄ nanocomposites with enhanced adsorptional photocatalytic activity for methylene blue degradation, *Int. J. Photoenergy* 2013 (2013), Article ID 726250.
- [23] B. Pare, S.B. Jonnalagadda, H. Tomar, P. Singh, V.W. Bhagwat, ZnO assisted photocatalytic degradation of acridine orange in aqueous solution using visible irradiation, *Desalination* 232 (2008) 80–90.
- [24] B. Pare, P. Singh, S.B. Jonnalagadda, Degradation and mineralization of Victoria blue B dye in a slurry photoreactor using advanced oxidation process, *J. Sci. Ind. Res.* 68 (2009) 724–729.
- [25] B. Pare, P. Singh, S.B. Jonnalagadda, Visible light-driven photocatalytic degradation and mineralization of neutral red dye in slurry photoreactor, *Indian J. Chem. Technol.* 17 (2010) 391–395.
- [26] C. Yu, J.C. Yu, Sonochemical fabrication, characterization and photocatalytic properties of Ag/ZnWO₄ nanorod catalyst, *Mater. Sci. Eng. B* 169 (2009) 16–22.
- [27] C. Balazsi, Z. Kover, E. Horvath, C. Nemeth, Z. Kasztovszky, S.F. Kurunczi, Weber Examination of calcium-phosphate prepared from eggshell, *Mater. Sci. Forum* 537–538 (2007) 105–112.
- [28] D. Li, R. Shi, C. Pan, Y. Zhu, H. Zhao, Influence of ZnWO₄ nanorod aspect ratio on the photocatalytic activity, *Cryst. Eng. Commun.* 13 (2011) 4695–4700.
- [29] W.T. Tsai, J.M. Yang, C.W. Lai, Y.H. Cheng, C.C. Lin, C.W. Yeh, Characterization and adsorption properties of eggshells and eggshell membrane, *Bioresour. Technol.* 97 (2006) 488–493.
- [30] A. Roy, J. Bhattacharya, Microwave assisted synthesis and characterization of CaO nanoparticles, *Int. J. Nanosci.* 10 (2011) 413–418.
- [31] S. Komarneni, R. Roy, Q.H. Li, Microwave-hydrothermal synthesis of ceramic powders, *Mater. Res. Bull.* 27 (1992) 1393–1405.
- [32] H.D. Xie, D.Z. Shen, X.Q. Wang, G.Q. Shen, Growth and characterization of KBi(WO₄)₂ single crystals, *Cryst. Res. Technol.* 42 (2007) 18–22.
- [33] G.B. Kumar, K. Sivaiah, S. Buddhudu, Synthesis and characterization of ZnWO₄ ceramic powder, *Ceram. Int.* 36 (2010) 199–202.
- [34] H.K. Shoun, S. Vigneswaran, H.H. Ngo, J.H. Him, Chemical coupling of photocatalysis with flocculation and adsorption in the removal of organic matter, *Water Res.* 39 (2006) 2549–2558.
- [35] C. Yu, J.C. Yu, Sonochemical fabrication: characterization and photocatalytic properties of Ag/ZnWO₄ nanorod catalyst, *Mater. Sci. Eng.* 169 (2009) 16–22.
- [36] C. Zhao, M. Pelaez, X. Duan, H. Deng, K.O. Shea, D.F. Kassinou, D.D. Dionysiou, Role of pH on photolytic and photocatalytic degradation of antibiotic oxytetracycline in aqueous solution under visible/solar light: kinetics and mechanism studies, *Appl. Catal. B* 134–135 (2013) 83–92.
- [37] G.V. Buxton, C. Greenstock, W.P. Hellman, A.B. Ross, Critical-review of rate constants for reactions of hydrated electrons, hydrogen-atoms and hydroxyl radicals ($\bullet\text{OH}/\bullet\text{O}^-$) in aqueous-solution, *J. Phys. Chem. Ref. Data* 17 (1988) 513–886.